



## ORIGINAL PAPER

**GPS/BDS TRIPLE-FREQUENCY CYCLE SLIP DETECTION AND REPAIR ALGORITHM BASED ON ADAPTIVE DETECTION THRESHOLD AND FNN-DERIVED IONOSPHERIC DELAY COMPENSATION**Nijia QIAN <sup>1,2)</sup>, Jingxiang GAO <sup>2)</sup>\*, Zengke LI <sup>2)</sup>, Fangchao LI <sup>2,3)</sup> and Cheng PAN <sup>1,2)</sup><sup>1)</sup> MNR Key Laboratory of Land Environment and Disaster Monitoring, China University of Mining and Technology, Xuzhou, China<sup>2)</sup> School of Environment Science and Spatial Informatics, China University of Mining and Technology, Xuzhou, China<sup>3)</sup> Nottingham Geospatial Institute, The University of Nottingham, Nottingham, UK\*Corresponding author's e-mail: [ts18160021a3tml@cumt.edu.cn](mailto:ts18160021a3tml@cumt.edu.cn)

## ARTICLE INFO

**Article history:**

Received 7 December 2019

Accepted 4 February 2020

Available online 16 April 2020

**Keywords:**

GPS

BDS

Triple-frequency cycle slip detection and repair

Geometry-free (GF)

Ionosphere-free (IF)

Ionospheric disturbances

Adaptive detection threshold

Feed-forward neural network (FNN)

## ABSTRACT

A refined triple-frequency cycle slip detection and repair algorithm for GPS/BDS undifferenced observables under high ionospheric disturbances is proposed. In this method, three linear-independent optimal observables combinations for GPS/BDS are selected. The residual ionospheric delay estimated from a “calculation-prediction mechanism”, namely flexibly determine whether to calculate delay by observables themselves or to predict delay by a feed-forward neural network (FNN), is used to compensate for the detection values. Additionally, we devise an adaptive detection threshold based on actual noise level to detect the cycle slip, and adopt the modified least-square decorrelation adjustment (MLAMBDA) to fix integer cycle slip. The performance of the proposed algorithm was tested with observables at 30 s sampling rate in a 2-day geomagnetic storm period. Results showed that the proposed algorithm can detect and repair all kinds of cycle slips as small as one cycle in the case of high ionospheric disturbances. No false repairs are generated despite the occurrence of very few misjudgments.

**1. INTRODUCTION**

It is widely known that based on high-precision carrier phase observables, GNSS has the capability of precise positioning and navigation both in static and dynamic applications, see e.g. (Cellmer et al., 2013; Li et al., 2015; Krzan and Przechodzinski, 2016). Examples are precise point positioning (PPP) and real-time kinematic (RTK) (Yu et al., 2016; Chen et al., 2018). However, in the cases of GNSS signal interruption, high ionospheric disturbances, high receiver dynamics, low signal-to-noise ratio (SNR), etc., cycle slip often occurs in carrier phase observables. Such a cycle slip breaks the continuity of the integer cycle counting in a continuous carrier tracking arc. Since one cycle of slip will cause about two decimeters of ranging error, and the size of that can change from one to millions of cycles, it significantly affects the precision and reliability of high-precision navigation and positioning (Kim et al., 2015; Zangeneh-Nejad et al., 2017). As a result, cycle slip detection and repair must be correctly dealt with before GNSS data processing.

The modern GPS, BDS, and Galileo have begun to broadcast triple-frequency or multi-frequency signals (Huang et al., 2016; Chang et al., 2018). The emergence of additional frequencies brings more freedom to the combination of observables with large

wavelengths, small measurement noise, and weak ionospheric delay, which could significantly improve the success rate of integer ambiguity and cycle slip processing (Zeng et al., 2018). Detecting and repairing cycle slip with triple-frequency combining signals simply employs time-differenced method, see e.g. (de Lacy et al., 2012; Zhang and Li, 2016; Tian et al., 2019). The demerit of these methods is that the effect of ionospheric delay is not taken into consideration, so they are only applicable to the cases of stable ionospheric activities or high sampling rate. Once ionospheric disturbances are active and sampling interval is large, it is easy to generate leakage judgments or misjudgments due to the interference of large residual ionospheric delay or measurement noise.

Ionospheric delay modelling is a constant challenge in geodesy, meteorology and communication science etc. (Rocken et al., 2000; Conker et al., 2003; Wu et al., 2013). Although there have been a wide variety of ionospheric models, it is still difficult to apply them to cycle slip detection and repair due to their complexity, resolution and so on, especially none for real-time applications. In order to tackle the problem of ionospheric delay, Chen and Zhang (2016) used three GF phase combinations to eliminate the first-order and second-order ionospheric delay, but the

large combination coefficients would significantly amplify the measurement noise. Gao et al. (2018) combined extra-wide lane (EWL), wide lane (WL), and narrow lane (NL) to detect and repair cycle slip, but compensation for residual ionospheric delay was only applied to the NL observables. The observables of EWL and WL were still suffered from the ionospheric delay. Yao et al. (2016) proposed to take the mean value of the residual ionospheric delay from several previous epochs to compensate for the current epoch; however, this was not applicable to severe ionospheric disturbances conditions between adjacent epochs. (Li et al. (2018), Chang et al. (2019) and Li et al. (2019) put forward the method in which polynomial interpolation fitting was applied to the residual ionospheric delay of the previous epochs, and a prediction was made using extrapolation to compensate for the current epoch, but Runge phenomenon is easily generated at polynomial interpolation node.

In this paper, the double-time-differenced residual ionospheric delay, rather than single-time-differenced one in previous methods, is estimated utilizing a “calculation-prediction mechanism” and then compensated for detection values. In this mechanism, a set of pre-determined conditions firstly judge whether there are some cycle slips at current epoch. If there is no cycle slip or a cycle slip only occurs at one frequency, the rest of frequencies’ signals could still be used to calculate the double-time-differenced residual ionospheric delay. As cycle slips happen at two or three frequencies, a nonlinear fitter, namely a feed-forward neural network (FNN), is employed to make extrapolations for ionospheric delay. This is based on the sparsity of cycle slips, which means that it is beyond the realms of possibility that most of the epochs exist cycle slips (Li et al., 2016; Li et al., 2017). This sparsity makes it possible for FNN to fit for ionospheric delay of the neighboring epochs. Another problem exists in cycle slip processing is that the standard deviation of the code and carrier phase observables noise are usually set to 0.3 m and 0.003 m, respectively, so as to calculate the fixed detection thresholds (Wu et al., 2010; Yao et al., 2016), which may generate misjudgments or leakage judgments as measurement surroundings change. Therefore, to reduce the effect of extrapolation error and to adapt to other measurement noise including stochastic noise, multipath and so on, a reliable but simple detection threshold is promising. In this work, based on statistic information of detection values and residual ionospheric delay of previous epochs, an adaptive threshold is constructed for cycle slip detection.

The rest of the paper is organized as follows. Section 2 is devoted to terminology introduction and problem formulation. In this section, the construction of three optimal triple-frequency observables combination and integer estimation of cycle slips are introduced. The main methodology is developed in Section 3. In its two subsections, the details of “calculation-prediction mechanism”, adaptive detection thresholds are presented, respectively.

Section 4 shows the performance of the proposed algorithm for simulated cycle slips and real cycle slips, and concluding remarks are presented in Section 5.

## 2. PROBLEM FORMULATION

### 2.1. BASIC OBSERVABLE EQUATIONS

Ignoring the influence of second-order and higher-order ionospheric delay, GNSS code and carrier phase observation equations can be expressed by Eqs. (1) and (2) (Qian et al., 2019):

$$P_{r,i}^s(k) = \rho_r^s(k) + c[dt_r(k) - dt^s(k)] + b_{r,i}^s(k) + T_r^s(k) + K_i I_{r,1}^s(k) + \zeta_{r,i}^s(k) \quad (1)$$

$$\lambda_i \varphi_{r,i}^s(k) = \rho_r^s(k) + c[\delta t_r(k) - \delta t^s(k)] + B_{r,i}^s(k) + \lambda_i N_{r,i}^s(k) + T_r^s(k) - K_i I_{r,1}^s(k) + \lambda_i \xi_{r,i}^s(k) \quad (2)$$

where  $P$  is code observables in meters, and  $\varphi$  is carrier phase observables in cycles, corresponding to carrier wavelength  $\lambda$ . The superscript  $s$  and the subscripts  $r$  and  $i$  represent indices of satellite, receiver, and frequency, respectively, and  $k$  represents epoch index. The symbol  $\rho$  refers to distance of line-of-sight vector between satellite and receiver;  $dt$  refers to clock bias of code observables;  $\delta t$  refers to clock bias of carrier phase observables, and  $c$  represents transmission speed of light in vacuum. The parameters  $b_i$  and  $B_i$  indicate hardware delay of the code and carrier phase observables (including satellite’s and receiver’s). The parameter  $T$  is tropospheric delay,  $I_1$  is ionospheric delay on the first frequency, and  $K_i = f_1^2 / f_i^2$  represents amplification factor of ionospheric delay.  $N_i$ ,  $\zeta_i$  and  $\xi_i$  denote integer ambiguity, measurement noise of code, and carrier phase observables, respectively. It is reasonable to consider that measurement noise is related to frequency and subject to the normal distribution, with a mean of zero and standard deviation of  $\sigma_P$  and  $\sigma_\varphi$ , satisfying  $\sigma_{P_1} = \sigma_{P_2} = \sigma_{P_3} = \sigma_P$  and  $\sigma_{\varphi_1} = \sigma_{\varphi_2} = \sigma_{\varphi_3} = \sigma_\varphi$ .

In order to simplify expression, the indices of satellite, receiver, and epoch are omitted. When a cycle slip occurs between two adjacent epochs, the single-time-differenced (STD) observation model is shown as Eqs. (3) and (4):

$$\Delta P_i = \Delta \rho + c(\Delta dt_r - \Delta dt^s) + \Delta T + K_i \Delta I_1 + \Delta \zeta_i \quad (3)$$

$$\lambda_i \Delta \varphi_i = \Delta \rho + c(\Delta \delta t_r - \Delta \delta t^s) + \Delta T - K_i \Delta I_1 + \lambda_i \Delta N_i + \lambda_i \Delta \xi_i \quad (4)$$

where  $\Delta$  represents time-differenced operator,  $\Delta N_i$  refers to cycle slip of carrier phase observables on  $i$ th frequency, and the remaining symbols are the same as above. Note that hardware delay terms can be completely removed due to their stability over a short time span, and so is inter-observation-type bias (IOTB) between code and carrier phase observables, resulting in  $\Delta dt = \Delta \delta t$  (Teunissen and de Bakker, 2013).

## 2.2. CODE-PHASE COMBINATION

According to triple-frequency theory, the STD forms of triple-frequency code combination and carrier phase combination can be expressed by Eqs. (5) and (6) (Yao et al., 2016):

$$\begin{aligned}\Delta P_{abc} &= a\Delta P_1 + b\Delta P_2 + c\Delta P_3 \\ &= \Delta\rho + c(\Delta dt_r - \Delta dt^s) + \Delta T + K_{abc}\Delta I_1 + \Delta\zeta_{abc}\end{aligned}\quad (5)$$

$$\begin{aligned}\lambda_{ijk}\Delta\varphi_{ijk} &= \lambda_{ijk}(i\Delta\varphi_1 + j\Delta\varphi_2 + k\Delta\varphi_3) \\ &= \Delta\rho + c(\Delta dt_r - \Delta dt^s) + \Delta T - K_{ijk}\Delta I_1 + \\ &+ \lambda_{ijk}\Delta N_{ijk} + \lambda_{ijk}\Delta\xi_{ijk}\end{aligned}\quad (6)$$

with

$$K_{abc} = a + b\left(\frac{f_1^2}{f_2^2}\right) + c\left(\frac{f_1^2}{f_3^2}\right), \quad K_{ijk} = \frac{\lambda_{ijk}}{\lambda_1}\left(i + j\frac{\lambda_2}{\lambda_1} + k\frac{\lambda_3}{\lambda_1}\right)$$

$$\lambda_{ijk} = \frac{\lambda_1\lambda_2\lambda_3}{(i\lambda_2\lambda_3 + j\lambda_1\lambda_3 + k\lambda_1\lambda_2)},$$

$$\Delta N_{ijk} = i\Delta N_1 + j\Delta N_2 + k\Delta N_3,$$

$$\Delta\zeta_{abc} = a\Delta\zeta_1 + b\Delta\zeta_2 + c\Delta\zeta_3,$$

$$\Delta\xi_{ijk} = i\Delta\xi_1 + j\Delta\xi_2 + k\Delta\xi_3,$$

where  $\Delta P_{abc}$  and  $\Delta\varphi_{ijk}$  are code combination and carrier phase combination in STD forms, respectively, corresponding to combination wavelength  $\lambda_{ijk}$ . The code combination coefficients  $a$ ,  $b$  and  $c$ , meet the condition  $a+b+c=1$ , while the carrier phase combination coefficients  $i$ ,  $j$  and  $k$  should be integers to ensure the combination cycle slip is an integer.  $K_{abc}$  and  $K_{ijk}$  represent the ionospheric delay amplification factors of code combination and carrier phase combination.  $\Delta\zeta_{abc}$  and  $\Delta\xi_{ijk}$  represent their measurement noise, respectively.

By subtracting Eq. (6) from Eq. (5), the non-dispersive delay terms are eliminated, including the geometric distance, clock bias, and tropospheric delay. Then the detection value of the code-phase combination and its standard deviation are derived in Eqs. (7) and (8):

$$\begin{aligned}Detection_{code-phase} &= \Delta N_{ijk} = (\Delta\varphi_{ijk} - \Delta\xi_{ijk}) - \\ &- \frac{\Delta P_{abc} - \Delta\zeta_{abc}}{\lambda_{ijk}} + K_{abc,ijk}\Delta I_1\end{aligned}\quad (7)$$

$$\begin{aligned}\sigma_{code-phase} &= \\ &= \sqrt{2}\sqrt{(i^2 + j^2 + k^2)\sigma_\varphi^2 + (a^2 + b^2 + c^2)\sigma_P^2} / \lambda_{ijk}\end{aligned}\quad (8)$$

where  $K_{abc,ijk} = (K_{abc} + K_{ijk})/\lambda_{ijk}$  is ionospheric influence coefficient of code-phase combination. Note that the combination with longer wavelengths is less affected by noise of code observables, and rounding success rate is closely related to the standard deviation of detection value. So the combination with large wavelength namely  $\max(\lambda_{ijk})$ , high precision namely  $\min(\sigma_{code-phase})$  and weak ionospheric effect namely  $\min(K_{abc,ijk})$ , is the optimal one. It is obvious that  $a=b=c=1/3$  makes the code combination noise

smallest. Taking above factors into consideration, we selected (0, 1, -1) for GPS and (0, -1, 1) for BDS phase combination coefficients, which is consistent with the conclusion in (Cocard et al., 2008).

Note that first-order ionospheric delay still exists after between-epoch difference. For stable ionospheric activities, one can select the combination with small  $K_{abc,ijk}$  to ignore the influence of residual ionospheric delay; however, for the case of active ionospheric disturbances, residual ionospheric delay is relatively large, and directly ignoring its influence may lead to leakage judgments or misjudgments. In this paper, only the latter case is studied. When residual ionospheric delay reaches 0.02 m, the success rate of rounding cycle slip estimation is just 97 % (Liu et al., 2018). Therefore, we suggest compensating residual ionospheric delay for detection values. This will be discussed in Section 3.

## 2.3. GF PHASE COMBINATION

A single code-phase combination cannot detect all kinds of cycle slip. It is necessary to construct another two linearly independent observable combinations to detect insensitive cycle slips. Assuming that  $\alpha$ ,  $\beta$ , and  $\gamma$  (satisfying  $\alpha+\beta+\gamma=0$ ) are coefficients of GF phase combination, then its STD form is shown in Eq. (9) (Yao et al., 2016):

$$\begin{aligned}\Delta L_{\alpha\beta\gamma} &= \alpha\lambda_1\Delta\varphi_1 + \beta\lambda_2\Delta\varphi_2 + \gamma\lambda_3\Delta\varphi_3 \\ &= \Delta N_{\alpha\beta\gamma} - K_{\alpha\beta\gamma}\Delta I_1 / \lambda_1 + \Delta\xi_{\alpha\beta\gamma}\end{aligned}\quad (9)$$

with

$$\Delta N_{\alpha\beta\gamma} = \alpha\lambda_1\Delta N_1 + \beta\lambda_2\Delta N_2 + \gamma\lambda_3\Delta N_3,$$

$$K_{\alpha\beta\gamma} = \alpha\lambda_1 + \beta(\lambda_2^2 / \lambda_1) + \gamma(\lambda_3^2 / \lambda_1),$$

$$\Delta\xi_{\alpha\beta\gamma} = \alpha\lambda_1\Delta\xi_1 + \beta\lambda_2\Delta\xi_2 + \gamma\lambda_3\Delta\xi_3,$$

where  $\Delta L_{\alpha\beta\gamma}$  represents GF phase combination in STD form,  $\Delta N_{\alpha\beta\gamma}$  represents combination cycle slip,  $K_{\alpha\beta\gamma}$  refers to amplification coefficient of ionospheric delay, and  $\Delta\xi_{\alpha\beta\gamma}$  is measurement noise of GF phase combination.

The influence of residual ionospheric delay can be further weakened by using double-time-difference (DTD) between three consecutive epochs, thus deriving the detection value of GF phase combination and its standard deviation, as shown in Eqs. (10) and (11):

$$\begin{aligned}Detection_{GF} &= \Delta\nabla N_{\alpha\beta\gamma} = \Delta\nabla L_{\alpha\beta\gamma} + K_{\alpha\beta\gamma}\Delta\nabla I_1 / \lambda_1 \\ &- \Delta\nabla\xi_{\alpha\beta\gamma} = \\ &= \alpha\lambda_1\Delta\nabla\varphi_1 + \beta\lambda_2\Delta\nabla\varphi_2 + \gamma\lambda_3\Delta\nabla\varphi_3 + \\ &+ K_{\alpha\beta\gamma}\Delta\nabla I_1 / \lambda_1 - \Delta\nabla\xi_{\alpha\beta\gamma}\end{aligned}\quad (10)$$

$$\sigma_{GF} = 2\sqrt{(\alpha\lambda_1)^2 + (\beta\lambda_2)^2 + (\gamma\lambda_3)^2}\sigma_\varphi\quad (11)$$

where  $\Delta\nabla$  represents DTD operator. The DTD operation between three epochs amplifies the measurement noise of detection value, but considering

that GF phase combination completely adopts high-precision phase observables, this influence can be ignored. Moreover, the difference between three epochs significantly weakens the residual ionosphere delay, which is generally less than 0.01 m under ordinary circumstances. We choose the optimal coefficients by imposing conditions  $\min(K_{\alpha\beta\gamma})$  and  $\min(\sigma_{GF})$ . As a result, the combinations (1, -1, 0) for GPS and (1, 0, -1) for BDS are adopted.

#### 2.4. GFIF PHASE COMBINATION

GFIF phase combination is different from GF phase combination, which adopts an STD model since the first-order ionospheric delay has been completely eliminated, and its cycle slip detection quantity and standard deviation can be expressed as Eqs. (12) and (13) (Pu and Xiong, 2019):

$$\begin{aligned} \text{Detection}_{GFIF} &= \Delta L_{\omega\theta\epsilon} + K_{\omega\theta\epsilon} \Delta I_1 / \lambda_1 - \Delta \xi_{\omega\theta\epsilon} \\ &= \omega \lambda_1 \Delta \varphi_1 + \theta \lambda_2 \Delta \varphi_2 + \epsilon \lambda_3 \Delta \varphi_3 + \\ &\quad + K_{\omega\theta\epsilon} \Delta I_1 / \lambda_1 - \Delta \xi_{\omega\theta\epsilon} \end{aligned} \quad (12)$$

$$\sigma_{GFIF} = \sqrt{2} \sqrt{(\omega \lambda_1)^2 + (\theta \lambda_2)^2 + (\epsilon \lambda_3)^2} \sigma_{\varphi} \quad (13)$$

with

$$\begin{aligned} \Delta N_{\omega\theta\epsilon} &= \omega \lambda_1 \Delta N_1 + \theta \lambda_2 \Delta N_2 + \epsilon \lambda_3 \Delta N_3, \\ K_{\omega\theta\epsilon} &= \omega \lambda_1 + \theta (\lambda_2^2 / \lambda_1) + \epsilon (\lambda_3^2 / \lambda_1), \\ \Delta \xi_{\omega\theta\epsilon} &= \omega \lambda_1 \Delta \xi_1 + \theta \lambda_2 \Delta \xi_2 + \epsilon \lambda_3 \Delta \xi_3, \end{aligned}$$

where  $\Delta L_{\omega\theta\epsilon}$  represents GFIF phase combination observables in STD form,  $\Delta N_{\omega\theta\epsilon}$  represents combination cycle slip. Here we select the optimal combination utilizing the following conditions: the first is the eliminations of geometric distance and ionospheric delay, namely  $\omega + \theta + \epsilon = 0$  and  $K_{\omega\theta\epsilon} = 0$ ; the second is the precision ensurance of detection quantity, namely  $\sigma_{GFIF} \leq T_{\sigma}$ , where  $T_{\sigma}$  is an empirically determined threshold; the last one is ability to detect small cycle slips, namely  $\omega \lambda_1 > \mu \sigma_{GFIF}$ ,  $\theta \lambda_1 > \mu \sigma_{GFIF}$  and  $\epsilon \lambda_1 > \mu \sigma_{GFIF}$ . To avoid the amplification of measurement noise, we search for the value of  $\omega$  between [0.1, 1.0] with a step size of 0.0001 and finally determined (0.2022, -1.0962, 0.8940) for GPS and (0.2709, 0.8825, -1.1534) for BDS GFIF combination.

#### 2.5. INTEGER ESTIMATION OF CYCLE SLIP

According to above statements, we select code-phase combination  $(i, j, k)$ , GF phase combination  $(\alpha, \beta, \gamma)$ , and GFIF phase combination  $(\omega, \theta, \epsilon)$  to construct three linearly independent detection quantities. In order to facilitate calculation, the unit of code-phase combination is converted into meters, and Eq. (14) can be established based on the relationship between combination observables and original observables.

$$\begin{aligned} L_{3 \times 1} &= B_{3 \times 6} K_{6 \times 1} = \\ &= \begin{bmatrix} i \lambda_{ijk} & j \lambda_{ijk} & k \lambda_{ijk} & -a & -b & -c \\ \alpha \lambda_1 & \beta \lambda_2 & \gamma \lambda_3 & 0 & 0 & 0 \\ \omega \lambda_1 & \theta \lambda_2 & \epsilon \lambda_3 & 0 & 0 & 0 \end{bmatrix} \times \begin{bmatrix} \Delta \varphi_1 \\ \Delta \varphi_2 \\ \Delta \varphi_3 \\ \Delta P_1 \\ \Delta P_2 \\ \Delta P_3 \end{bmatrix} \end{aligned} \quad (14)$$

where  $\Delta \varphi_i$  and  $\Delta P_i$  refer to original observables in STD forms. Assuming there is a cycle slip  $(\Delta N_1, \Delta N_2, \Delta N_3)$  on three frequencies at an epoch, we can derive the relationship between combination cycle slip and original cycle slip, as shown in Eq. (15):

$$A_{3 \times 3} \Delta z_{3 \times 1} = L_{3 \times 1} \quad (15)$$

with

$$\begin{aligned} A_{3 \times 3} &= \begin{bmatrix} i \lambda_{ijk} & j \lambda_{ijk} & k \lambda_{ijk} \\ \alpha \lambda_1 & \beta \lambda_2 & \gamma \lambda_3 \\ \omega \lambda_1 & \theta \lambda_2 & \epsilon \lambda_3 \end{bmatrix}, \Delta z_{3 \times 1} = \begin{bmatrix} \Delta N_1 \\ \Delta N_2 \\ \Delta N_3 \end{bmatrix}, \\ L_{3 \times 1} &= \begin{bmatrix} \Delta \hat{N}_{(i,j,k)} \\ \Delta \hat{N}_{(\alpha,\beta,\gamma)} \\ \Delta \hat{N}_{(\omega,\theta,\epsilon)} \end{bmatrix}, \end{aligned}$$

where  $A_{3 \times 3}$ ,  $\Delta z_{3 \times 1}$ , and  $L_{3 \times 1}$  are design matrix, cycle slip, and detection value, respectively. Due to integer characteristics of code-phase combination cycle slip,  $\Delta \hat{N}_{(i,j,k)}$  is the rounding result after compensating for the residual ionospheric delay, while  $\Delta \hat{N}_{(\alpha,\beta,\gamma)}$  is the result after applying correction for the residual ionospheric delay. Then, the least squares solution of original cycle slip can be obtained, as shown in Eq. (16):

$$\begin{aligned} \Delta \bar{z} &= (A^T Q_{LL}^{-1} A)^{-1} A^T Q_{LL}^{-1} L \\ &= A^{-1} L. \end{aligned} \quad (16)$$

Using Eq. (19), float solution of cycle slip  $\Delta \bar{z}$  can be obtained. Now cycle slip repair turns into the problem of fixing it. Similar to (Pu and Xiong, 2019), we employ MLAMBDA algorithm proposed by (Chang et al., 2005), which is devised to search the integer vector  $\Delta \bar{z}$  closest to float vector  $\Delta \bar{z}$  according to objective function given by Eq. (17):

$$\min[(\Delta \bar{z} - \Delta \bar{z}) Q_{\Delta \bar{z}}^{-1} (\Delta \bar{z} - \Delta \bar{z})] \quad (17)$$

where  $Q_{\Delta \bar{z}}$  denotes standard deviation of cycle slip, derived from detection values and residual ionospheric delay of previous epochs, whose deviation will be introduced in Section 3.

### 3. METHODOLOGY

The introduction of methodology is split into two parts in this section. The details of ‘‘calculation-

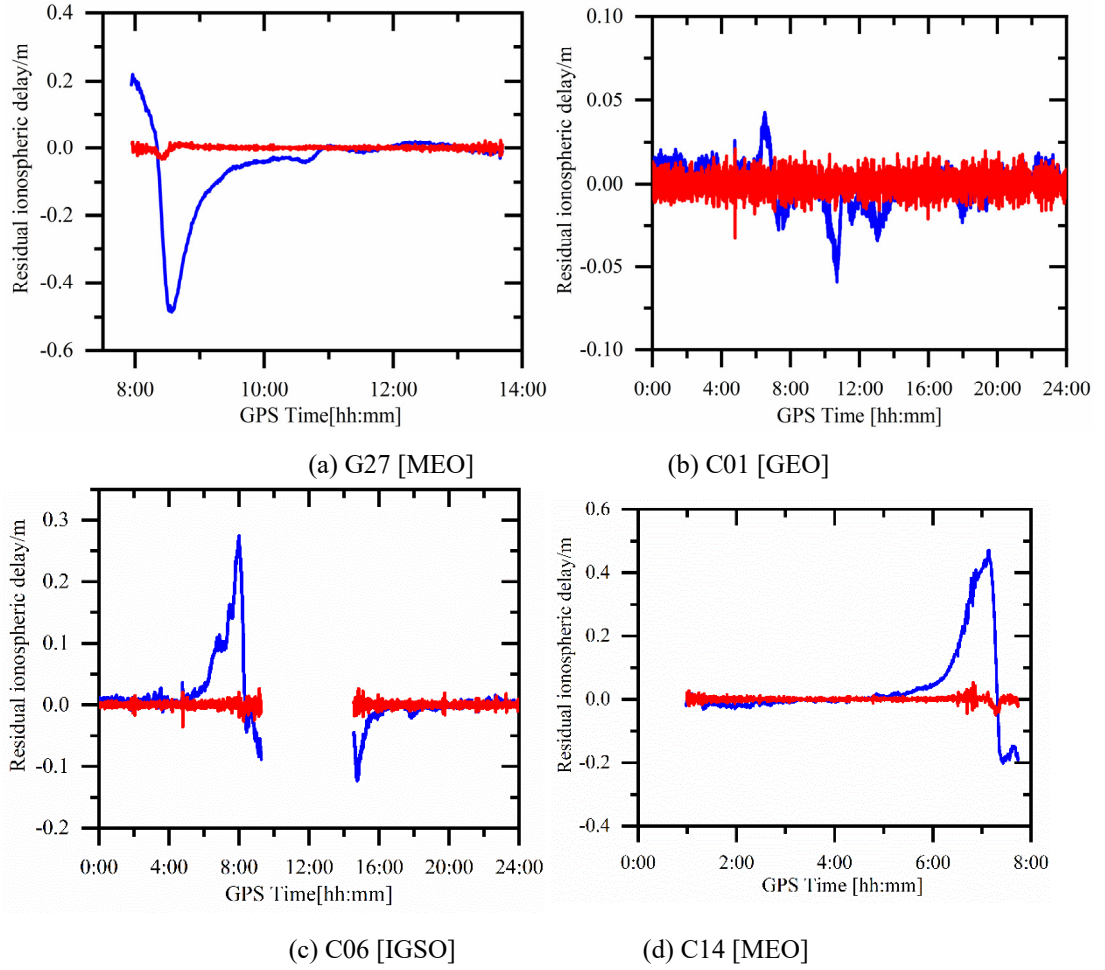


**Fig. 1** Residual ionospheric delay at JFNG station on 17 March, 2018 (Red represents  $\Delta I_1$ , and Blue represents  $\Delta \nabla I_1$ ).

prediction mechanism” for estimating residual ionospheric delay are introduced in Section 3.1. The adaptive detection threshold is detailed in Section 3.2.

### 3.1. CALCULATION-PREDICTION MECHANISM

Assuming there is no cycle slip between three consecutive epochs or a cycle slip exists but has been repaired, we can obtain  $\Delta I_1$  from Eqs. (18) to (20), where the superscripts 12, 13, and 23 represent that carrier phase observables on corresponding two frequencies are used. Theoretically, when ionosphere is active,  $\Delta I_1$  will fluctuate violently over a large range within a short period, so it is difficult to find the change rule. However,  $\Delta \nabla I_1$ , whose deviation is shown as Eq. (21), is smaller with more gradual changes. And there may be a numerical difference of one order of magnitude between them, which means the prediction error of the latter would be significantly smaller than that of the former. Figure 1 shows the comparison between  $\Delta I_1$  and  $\Delta \nabla I_1$  in a period of geomagnetic storm, which demonstrate the above hypothesis. Although the  $\Delta \nabla I_1$  in each figure looks like a random series, it would be possible to make

prediction for this due to correlation between previous epochs. There are several reasons for this correlation. First, the measurement environment can be approximately considered to be constant in a short period of time, which means the residual ionospheric delay would remain at a stable level (or within a small magnitude). Second, ionospheric delay is closely related to SNR and satellite elevation mask. By the epoch goes on, the SNR and satellite elevation mask will change correspondingly, thus make the residual ionospheric delay change together. In this manner, the SNR and elevation mask can be used as media between epochs. So, it would be better to make predictions for  $\Delta \nabla I_1$  rather than  $\Delta I_1$ .

$$\Delta I_1^{12}(n, n-1) = \frac{\lambda_1 \Delta \varphi_1(n, n-1) - \lambda_2 \Delta \varphi_2(n, n-1)}{f_1^2 / f_2^2 - 1} \quad (18)$$

$$\Delta I_1^{13}(n, n-1) = \frac{\lambda_1 \Delta \varphi_1(n, n-1) - \lambda_3 \Delta \varphi_3(n, n-1)}{f_1^2 / f_3^2 - 1} \quad (19)$$

$$\Delta I_1^{23}(n, n-1) = \frac{\lambda_2 \Delta \varphi_2(n, n-1) - \lambda_3 \Delta \varphi_3(n, n-1)}{\frac{f_2^2}{f_3^2 - 1}} \frac{f_2^2}{f_1^2} \quad (20)$$

$$\Delta\nabla I_1(n, n-1, n-2) = \Delta I_1(n, n-1) - \Delta I_1(n-1, n-2) \quad (21)$$

We assume that there is no cycle slip before current epoch or the cycle slip exists but has been repaired, and current epoch index is  $n$ . If a cycle slip occurs at current epoch, the  $\Delta\nabla I_1$  calculated by Eq. (21) would be significantly larger than normal value. Based on this rule, we design the following specific steps to predict  $\Delta\nabla I_1$  for current epoch, shown as follows:

**Step 1:** Calculate  $\Delta\nabla I_1^{12}$ ,  $\Delta\nabla I_1^{13}$  and  $\Delta\nabla I_1^{23}$  by Eqs. (18)–(21), and the mean and standard deviation of  $\Delta\nabla I_1$  from  $m$  previous epochs by Eqs. (22) and (23):

$$\sigma_{\Delta\nabla I_1} = \text{std}(\Delta\nabla I_1 \Big|_{n-m}^{n-1}) \quad (22)$$

$$\overline{\Delta\nabla I_1} = \text{mean}(\Delta\nabla I_1 \Big|_{n-m}^{n-1}). \quad (23)$$

**Step 2:** Condition judgment. If conditions (1), (2), and (3) are met at the same time, it means that there is no cycle slip at current epoch, so we take  $\Delta\nabla\hat{I}_1 = \Delta\nabla I_1^{12}$  and then go straight to Step 5. If condition (1) is satisfied while conditions (2) and (3) are not satisfied, it means that there is a cycle slip on the third frequency with  $\Delta\nabla I_1^{13}$  and  $\Delta\nabla I_1^{23}$  incredible, so we take  $\Delta\nabla\hat{I}_1 = \Delta\nabla I_1^{12}$  and then go straight to Step 5. If condition (2) is satisfied while conditions (1) and (3) are not satisfied, it means that there is a cycle slip on the second frequency with  $\Delta\nabla I_1^{12}$  and  $\Delta\nabla I_1^{23}$  incredible, so we take  $\Delta\nabla\hat{I}_1 = \Delta\nabla I_1^{13}$  and then go straight to Step 5. If condition (3) is satisfied while conditions (1) and (2) are not satisfied, it means that there is a cycle slip on the first frequency with  $\Delta\nabla I_1^{12}$  and  $\Delta\nabla I_1^{13}$  incredible, so we take  $\Delta\nabla\hat{I}_1 = \Delta\nabla I_1^{23}$  and then go straight to Step 5. Otherwise, we consider more than one frequency exists cycle slip, and residual ionospheric delay cannot be calculated from observables, so we execute Step 3 to make a prediction.

$$\text{Condition (1): } \left| \Delta\nabla I_1^{12}(n, n-1, n-2) - \overline{\Delta\nabla I_1} \right| < \mu\sigma_{\Delta\nabla I_1} \quad (24)$$

$$\text{Condition (2): } \left| \Delta\nabla I_1^{13}(n, n-1, n-2) - \overline{\Delta\nabla I_1} \right| < \mu\sigma_{\Delta\nabla I_1} \quad (25)$$

$$\text{Condition (3): } \left| \Delta\nabla I_1^{23}(n, n-1, n-2) - \overline{\Delta\nabla I_1} \right| < \mu\sigma_{\Delta\nabla I_1} \quad (26)$$

where  $\mu$  denotes the threshold coefficient. Here we take  $\mu=3$  corresponding to a 99.7% confidence level.

**Step 3:** FNN fitting. The index of  $m$  previous epochs (1, 2, 3, ...,  $m$ ), satellite elevation mask of the  $(k-2)$ th,  $(k-1)$ th, and  $k$ th ( $n-m \leq k \leq n-1$ ) epochs, and signal noise ratio (SNR) of  $(k-2)$ th,  $(k-1)$ th, and  $k$ th epochs constitute training feature matrix  $\mathbf{P}$ , as shown in Eq. (27). The corresponding  $\Delta\nabla I_1$  of previous  $m$  epochs (calculated from the first and second frequencies) is used to form the training label matrix  $\mathbf{T}$  as given by Eq. (28). By learning from the training set composed of  $\mathbf{P}$  and  $\mathbf{T}$ , we can fit the nonlinear mapping model of  $m$  neighboring  $\Delta\nabla I_1$ :

$$\mathbf{P} = \begin{bmatrix} n-m & n-m+1 & \dots & n-1 \\ \text{Elv}(n-m-2) & \text{Elv}(n-m-1) & \dots & \text{Elv}(n-3) \\ \text{Elv}(n-m-1) & \text{Elv}(n-m) & \dots & \text{Elv}(n-2) \\ \text{Elv}(n-m) & \text{Elv}(n-m+1) & \dots & \text{Elv}(n-1) \\ \text{SNR}(n-m-2) & \text{SNR}(n-m-1) & \dots & \text{SNR}(n-3) \\ \text{SNR}(n-m-1) & \text{SNR}(n-m) & \dots & \text{SNR}(n-2) \\ \text{SNR}(n-m) & \text{SNR}(n-m+1) & \dots & \text{SNR}(n-1) \end{bmatrix} \quad (27)$$

$$\mathbf{T} = \begin{bmatrix} \Delta\nabla I_1(n-m) & \Delta\nabla I_1(n-m+1) & \dots & \Delta\nabla I_1(n-1) \end{bmatrix} \quad (28)$$

**Step 4:** FNN extrapolation. We can obtain the extrapolated  $\Delta\nabla\hat{I}_1(n, n-1, n-2)$  by inputting the eigenvector expressed in Eq. (29) into fitted FNN model:

$$\mathbf{F} = [n \quad \text{Elv}(n-2) \quad \text{Elv}(n-1) \quad \text{Elv}(n) \quad \text{SNR}(n-2) \quad \text{SNR}(n-1) \quad \text{SNR}(n)]^T \quad (29)$$

**Step 5:** Compensate residual ionospheric delay for detection values.  $\Delta\nabla\hat{I}_1(n, n-1, n-2)$  is directly used to compensate for GF phase detection value. For code-phase combination,  $\Delta\hat{I}_1(n, n-1)$  is calculated by Eq. (30) and then compensated for its detection value:

$$\Delta\hat{I}_1(n, n-1) = \Delta I_1(n-1, n-2) + \Delta\nabla\hat{I}_1(n, n-1, n-2) \quad (30)$$

Then one can repeat above steps and move the window down to the last epoch. If the judgment conditions in Step 2 are satisfied, the calculated values are adopted; otherwise, the extrapolated values are used. Step 2 ensures that if a cycle slip occurs at a single frequency, the other two frequencies can be used to calculate the residual ionospheric delay, which can minimize estimation error. If more than one frequency exists cycle slip, the residual ionospheric delay can be extrapolated by FNN fitter, thus forming a “calculation-prediction mechanism”.

Note that the FNN used here, as shown in Figure 2, just needs to learn ionospheric characteristics in a previous neighboring period rather than a great quantity of training data, which can be regarded as a nonlinear fitter instead of polynomial fitting. The reason why we use elevation mask and SNR as training features is that they are both important indicators to evaluate quality of satellite signals and closely related to ionospheric delay. Furthermore,  $m$  should not be too large or too small. If we take a large  $m$ , the historical ionospheric information may be weak-correlated or uncorrelated to current epoch. If we take a small  $m$ , the FNN cannot learn the details of the ionospheric information fully. We take  $m=30$  empirically in this paper, which is enough for fitting neighboring ionospheric characteristics.

### 3.2. ADAPTIVE CYCLE SLIP DETECTION THRESHOLD

In most current cycle slip processing, the standard deviation of code and carrier phase observables are set as 0.3 m and 0.003 m, respectively, and then used to calculate a fixed threshold for cycle slip detection. In practice, the accuracy of detection quantities is related to a variety of factors, and fixed threshold of cycle slip detection is prone to generate misjudgments or leakage judgments with the changes of measurement surroundings and influence of ionospheric disturbances, especially for high-precision combinations of GF and GFIF. Therefore, it is necessary to determine an adaptive threshold.

An adaptive threshold for cycle slip detection based on actual noise level, namely the accuracy of detection values and activity level of ionosphere, is constructed. The standard deviation of cycle slip detection values can be calculated by historical detection values from previous  $m$  epochs, as shown in Eq. (31):

$$\sigma_{com} = std(Detection_{com} \Big|_{n-m}^{n-1}) \quad (31)$$

where the subscript *com* can represent code-phase combination, GF phase combination, and GFIF phase combination.

For code-phase combination, the compensation of the STD residual ionospheric delay can be decomposed into  $\Delta I_1(n, n-1) = \Delta I_1(n-1, n-2) + \Delta\nabla I_1(n, n-1, n-2)$ . Note that there is no error in  $\Delta I_1(n-1, n-2)$  because no cycle slip exists among previous epochs, and only  $\Delta\nabla I_1(n, n-1, n-2)$  has prediction error with standard deviation  $\sigma_{\Delta\nabla I_1}$ . Therefore, the detection threshold of code-phase combination can be determined by Eq. 32):

$$Threshold_{code-phase} = \mu \sqrt{\sigma_{code-phase}^2 + (K_{ijk} \sigma_{\Delta\nabla I_1} / \lambda_1)^2} \quad (32)$$

where  $\mu$  is threshold coefficient. Here we take  $\mu=4$  corresponding to a 99.9 % confidence level. Similarly, an adaptive detection threshold for GF combination can be constructed as shown in Eq. (33). For GFIF combination, since the first-order ionospheric delay has been eliminated and the influence of higher-order ionospheric delay is not considered, the detection threshold can be determined by Eq. (34):

$$Threshold_{GF} = \mu \sqrt{\sigma_{GF}^2 + (K_{\alpha\beta\gamma} \sigma_{\Delta\nabla I_1})^2} \quad (33)$$

$$Threshold_{GFIF} = \mu \sigma_{GFIF} \quad (34)$$

After adaptive detection thresholds are determined at current epoch, once any detection value exceeds the threshold, the existence of cycle slip at current epoch is determined. Note that the traditional fixed threshold is still employed at the initial several epochs. With the progress of cycle slip detection and repair, the detection threshold can be adjusted adaptively through learning from the previous epochs.

Based on above statements, the flowchart of the proposed algorithm is summarized in Figure 3. The residual ionospheric delay estimated by “calculation-prediction mechanism” is used to compensate for detection values of code-phase and GF phase combinations. Once a cycle slip is detected, its values will be fixed by MLAMBDA algorithm. Then the standard deviation of detection values and residual ionospheric delay will be updated automatically to prepare for the adaptive threshold and “calculation-prediction mechanism” of next epoch.





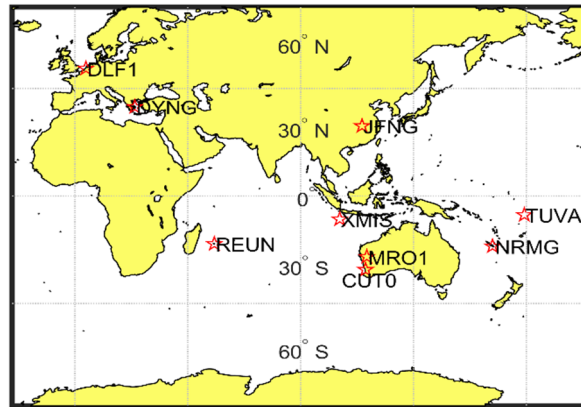


Fig. 4 Distribution of 9 MGEX stations.

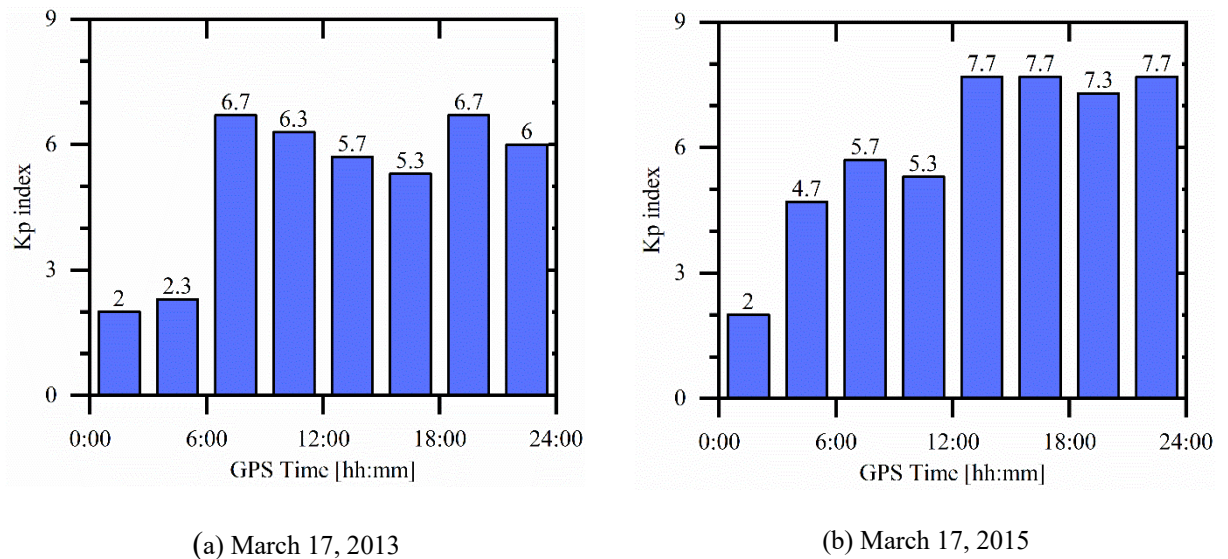


Fig. 5 Kp index of two geomagnetic storms.

including small cycle slips (denote by S), approximate cycle slips (denote by A), insensitive cycle slips (denote by I), consecutive cycle slips (denote by C) and random cycle slips (denote by R). Taking JFNG station as an example, the first four columns in Table 1 list detailed information of the added cycle slip.

Figures 6 and 7 show the results of cycle slip detection and repair. For clarity, we only present cycle slip detection values within the range of  $[-1, 1]$  cycles for code-phase combination,  $[-0.1, 0.1]$  meters for GF phase combination, and  $[-0.04, 0.04]$  meters for GFIF phase combination. From Figures 6 and 7, the followings are observed. First of all, all kinds of cycle slips can be detected by jointly using three combinations. Taking the G01 satellite in Figure 6(a) as an example, the code-phase combination is insensitive to  $(0, 3, 3)$  satisfying  $\Delta N_2 = \Delta N_3$  and  $(1, 0, 0)$  in which cycle slip only occurs on the first frequency, but they are both detectable for GF phase combination. The GF combination is insensitive to  $(32, 25, 0)$  satisfying  $\Delta N_1 = \Delta N_2 = \lambda_2 / \lambda_1 \approx 1.28$  and  $(0, 0, 1)$  in which only occurs at the third frequency, but the code-phase and GFIF phase combination can detect them. The

GFIF combination is insensitive to  $(1, 1, 1)$  which satisfies  $\Delta N_1 = \Delta N_2 = \Delta N_3$ , but the GF phase combination can detect it. In general, there is no insensitive cycle slip for three combinations, and all kinds of cycle slips can be detected.

Second, the changes of adaptive detection threshold also are shown in Figures 6 and 7. For code-phase combination, the adaptive detection threshold has a higher tense status than fixed threshold, but no misjudgment is generated. With regard to GF and GFIF phase combinations, taking Figure 6(b) as an example, the fixed threshold cannot accurately detect cycle slip due to the disturbances of ionosphere, resulting in a large number of misjudgments. However, the adaptive detection threshold adjusts automatically with the change of statistic information of detection values and residual ionospheric delay, which is obviously more in line with the actual situation. Third, since the angular velocity of MEO satellite is higher than that of IGSO and GEO satellites, the larger change in the satellite elevation mask means its measurement noise changes more significantly, and its adaptive detection threshold

**Table 1** The artificial added cycle slip and the result of cycle slip repair.

Date Station PRN (type)	Epoch	Cycle slip type	Values added	Float solution	Integer solution	Minimum residuals (R <sub>1st</sub> ,R <sub>2nd</sub> )
2013/03/17 JFNG G01(MEO)	13:40:00	S&I	(1,0,0)	(-0.11,-0.86,-0.86)	(1,0,0)	(2.71,27.70)
	14:20:00	S&I&P	(1,1,1)	(1.21,1.16,1.16)	(1,1,1)	(0.02,5.09)
	15:30:00	I&L	(32,25,0)	(31.91,24.92,-0.08)	(32,25,0)	(0.01,17.96)
	16:35:00	S&I	(0,3,3)	(0.26,3.22,3.22)	(0,3,3)	(0.08,30.09)
	17:20:00	S&I	(0,0,1)	(0.17,0.14,1.14)	(0,0,1)	(0.05,30.91)
	18:30:00	L&R	(-1,3,-6)	(-1.16,2.86,-6.14)	(-1,3,-6)	(0.02,9.13)
2013/03/17 JFNG C04(GEO)	02:00:00	S&I	(0,1,0)	(-0.01,0.99,-0.01)	(0,1,0)	(0.00,71.13)
	06:00:00	L&A	(-6,-6,-7)	(-6.16,-6.13,-7.13)	(-6,-6,-7)	(0.04,38.92)
	07:30:00	L&I	(123,0,100)	(123.03,0.00,100.00)	(123,0,100)	(0.07,54.02)
	12:10:00	S&I&P	(1,1,1)	(0.89,0.92,0.92)	(1,1,1)	(0.09,88.24)
	13:40:00	L&I	(0,5,5)	(-0.00,5.00,5.00)	(0,5,5)	(0.00,81.21)
	22:35:00	L&R	(59,83,41)	(59.06,83.05,41.05)	(59,83,41)	(0.01,48.61)
2013/03/17 JFNG C06(IGSO)	04:00:00	S&I	(0,0,1)	(0.01,0.01,1.01)	(0,0,1)	(0.00,89.08)
	06:00:00	S&A	(1,-2,1)	(0.88,-2.07,0.93)	(1,-2,1)	(0.29,64.00)
	08:00:00	S&I&P	(1,1,1)	(0.82,0.81,0.81)	(1,1,1)	(0.20,2.24)
	09:10:00	L&A	(14,13,13)	(14.33,13.28,13.28)	(14,13,13)	(0.04,2.17)
	16:40:00	L&I	(123,0,100)	(123.10,0.07,100.07)	(123,0,100)	(0.07,27.24)
	22:30:00	L&R	(1,53,238)	(1.14,53.11,238.11)	(1,53,238)	(0.06,53.77)
2013/03/17 JFNG C11(MEO)	15:00:00	S&I&P	(2,2,2)	(1.04,1.26,1.26)	(2,2,2)	(0.17,1.86)
	15:25:00	L&A	(11,12,11)	(11.67,12.59,11.59)	(11,12,11)	(0.06,0.45)
	18:00:00	L&R	(762,53,-3)	(762.40,53.31,-2.69)	(762,53,-3)	(0.14,13.56)
	20:10:00	S&P	(1,-1,0)	(1.06,-0.94,0.06)	(1,-1,0)	(0.01,10.92)
	22:10:00	L&R	(53,47,21)	(52.89,46.90,20.90)	(53,47,21)	(0.01,7.81)
	22:40:00	S&P	(-1,0,1)	(-1.14,-0.17,0.83)	(-1,0,1)	(0.09,0.39)
2015/03/17 JFNG G27 (MEO)	08:15:00	S&I&P	(1,1,1)	(0.90,0.91,0.91)	(1,1,1)	(0.00,2.24)
	08:45:00	L&A	(33,33,32)	(32.77,32.80,31.80)	(33,33,32)	(0.01,8.62)
	08:45:30	S&I&C	(0,1,1)	(-0.11,0.92,0.92)	(0,1,1)	(0.00,0.02)
	10:01:30	L&I	(32,25,0)	(32.17,25.13,0.13)	(32,25,0)	(0.02,22.94)
	11:45:00	S&I	(3,0,0)	(2.99,-0.03,-0.03)	(3,0,0)	(0.03,15.80)
	13:00:00	S&A	(-3,-2,-2)	(-3.06,-2.00,-2.00)	(-3,-2,-2)	(0.12,7.01)
2015/03/17 JFNG C01 (GEO)	04:14:00	S&I&P	(1,1,1)	(1.02,1.01,1.01)	(1,1,1)	(0.01,68.62)
	07:45:00	L&I	(123,0,100)	(123.16,0.18,100.18)	(123,0,100)	(0.06,0.39)
	11:05:00	L&I	(0,6,6)	(-0.13,5.86,5.86)	(0,6,6)	(0.09,1.30)
	11:05:30	S&I&C	(2,0,0)	(2.08,0.08,0.08)	(2,0,0)	(0.00,0.02)
	16:00:00	L&R	(46,73,-6)	(45.59,72.64,-6.36)	(46,73,-6)	(0.06,0.49)
	22:30:00	S&A	(3,2,3)	(2.98,2.00,3.00)	(3,2,3)	(0.04,55.52)
2015/03/17 JFNG C06 (IGSO)	03:21:30	S&I	(0,4,4)	(0.09,4.07,4.07)	(0,4,4)	(0.02,55.17)
	06:00:00	S&I	(1,0,0)	(0.99,0.00,0.00)	(1,0,0)	(0.01,26.11)
	06:56:30	S&I&C	(1,1,1)	(0.91,0.92,0.92)	(1,1,1)	(0.01,42.05)
	08:00:00	L&I	(0,10,0)	(-0.10,9.92,-0.08)	(0,10,0)	(0.00,13.92)
	15:15:00	L&I	(123,0,100)	(122.82,-0.15,99.85)	(123,0,100)	(0.01,8.27)
	22:28:30	L&R	(3,1,-560)	(3.04,1.05,-559.95)	(3,1,-560)	(0.04,4.98)
2015/03/17 JFNG C14 (MEO)	02:01:00	L&A	(54,54,53)	(54.38,54.32,53.32)	(54,54,53)	(0.06,13.73)
	05:00:00	L&R	(53,21,-1)	(53.06,21.03,-0.97)	(53,21,-1)	(0.05,18.05)
	06:00:00	S&I	(0,-1,0)	(-0.14,-1.12,-0.12)	(0,-1,0)	(0.02,25.47)
	06:39:00	S&I&P	(1,1,1)	(0.59,0.62,0.62)	(1,1,1)	(0.08,0.58)
	07:05:00	L&I	(-1,7,7)	(-0.82,7.20,7.20)	(-1,7,7)	(0.05,0.13)
	07:31:30	L&I	(1231,0,1000)	(1230.5,-0.48,999.5)	(1231,0,1000)	(0.02,0.07)

changes most violently among three kinds of orbit satellites. As a whole, the adaptive threshold is more reliable than fixed threshold, which will avoid neither misjudgments due to the excessively tense threshold nor leakage judgments due to the excessively loose threshold.

The last three columns in Table 1 list float solution and integer solution of cycle slip, as well as the corresponding minimum residual and

subminimum residual in cycle<sup>2</sup>. The following observations are made. First, all simulated cycle slips are correctly repaired, and the residual of optimal cycle slip is far less than that of suboptimal cycle slip. Second, if we directly round float cycle slip solutions, we cannot get correct integer solution in some cases. For example, direct rounding of the simulated cycle slip (1,0,0) in G01 on March 17, 2013, gives the wrong solution (0,-1,-1). However, MLAMBDA could fixed

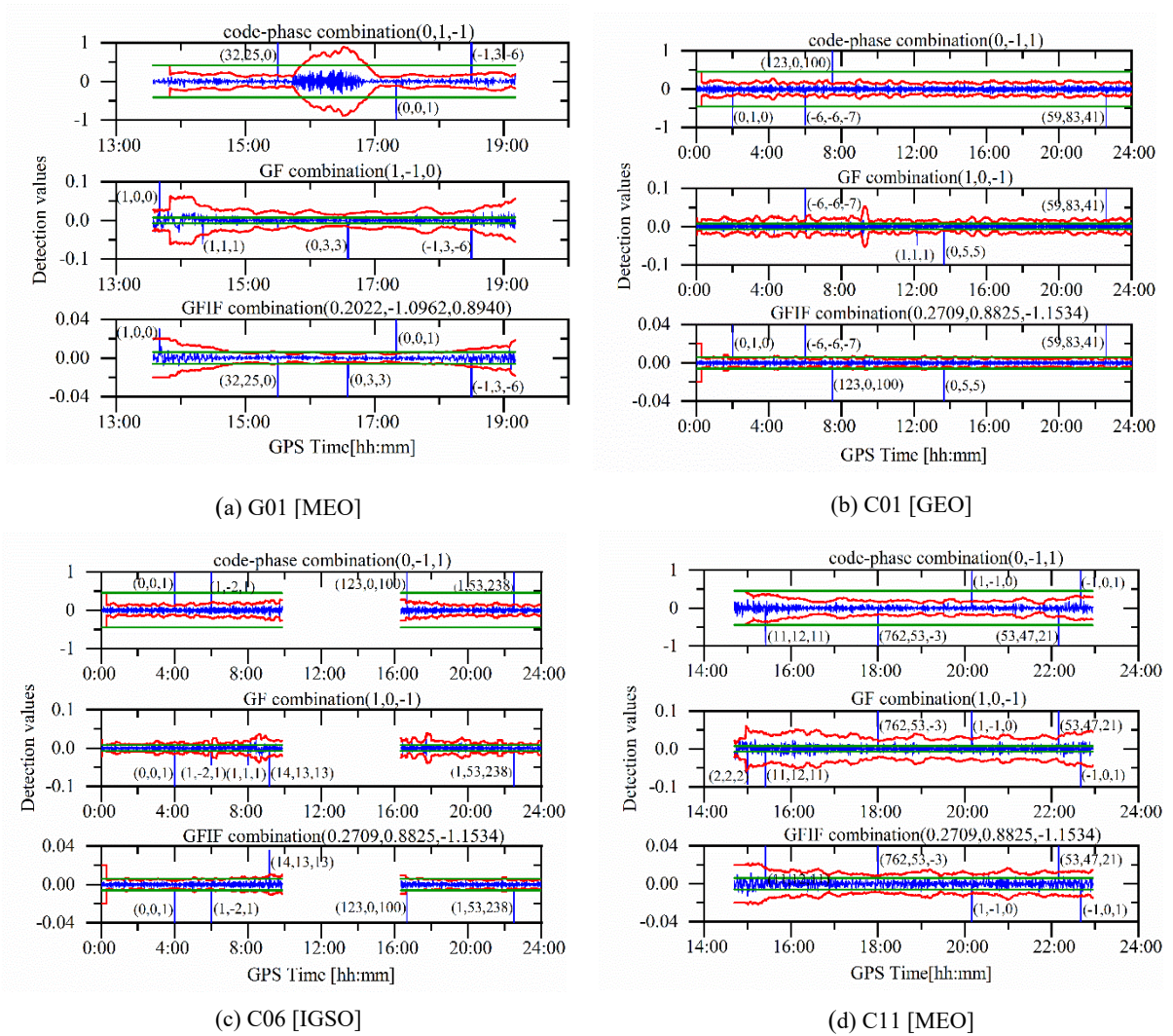


**Fig. 6** Detection and repair results of simulated cycle slip at JFNG station on March 17, 2013 (Blue represents detection values, Green represents fixed detection threshold and Red represents adaptive detection threshold.)

integer solution  $(1,0,0)$  correctly, which verified MLAMBDA is a reliable tool for fixing float cycle slips. Since few or no leakage judgment occurs under high ionospheric disturbances, we only show misjudgment rate of eight stations in Table 2. No cycle slip exists in original observables, and misjudgment rate is calculated by the ratio of misjudged epochs to total epochs. Results show that the proposed algorithm can maintain a detection success rate of more than 99.3%. Therefore, the proposed algorithm has a high reliability under ionospheric disturbances.

#### 4.2. REAL CYCLE SLIP DETECTION AND REPAIR EXPERIMENT

Ju et al. (2017) confirmed that due to constant relative position between receivers and BDS GEO satellites, cycle slip often occurs in GEO satellite observables. Since theoretical performance of IGSO and MEO satellites is similar to that of GEO, we only take GEO satellites as an example to test real cycle slip detection and repair performance.

We discovered that some cycle slips existed in

C05 observables tracked by CUT0 station on March 17, 2013, and C05 observables tracked by MRO1 station on March 17, 2015. For convenience, we call the former “CC05” satellite and the latter “MC05” satellite. Figure 8 shows residual ionospheric delay of these two satellites before cycle slip repaired. It is observed that residual ionospheric delay would keep at a low and relatively stable level when there is no cycle slip. Once cycle slips occur, they would significantly destroy this state. We can roughly determine that there is only a set of  $\pm 1$  cycle slips on the first and second frequencies, and several large cycles slips on the third frequency for CC05 satellite, while only  $\pm 1$  cycle slips exist on all frequencies for MC05 satellite.

Figure 9 shows cycle slip detection and repair results for CC05 and MC05 satellites. The epochs at which cycle slips are detected exactly correspond to epochs with outliers in Figure 8. In order to test the validity of the results, Figure 10 shows residual ionospheric delay after cycle slip repaired. After the cycle slip is detected and repaired,  $\Delta I_1$  only fluctuates

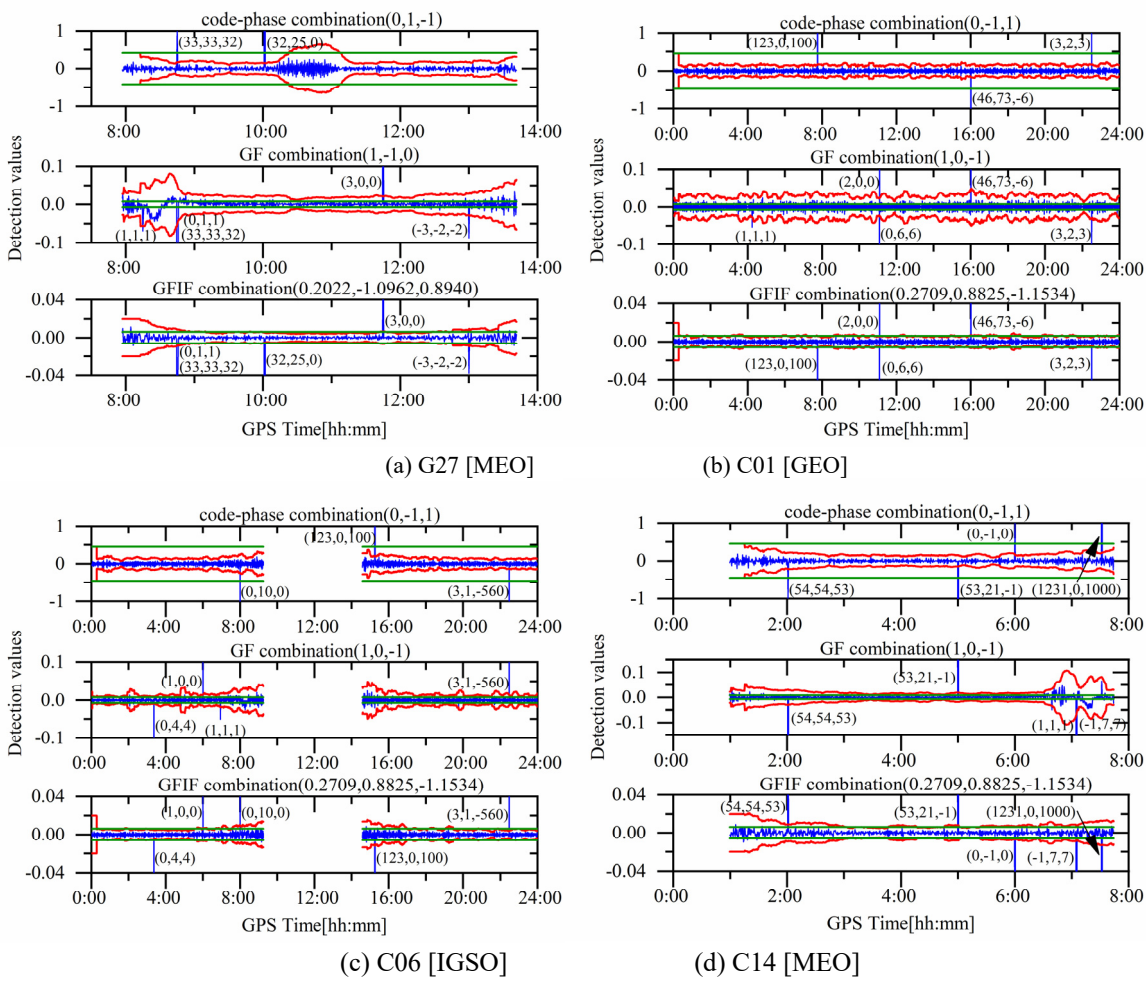


**Fig. 7** Detection and repair results of simulated cycle slip at JFNG station on March 17, 2015 (Blue represents detection values, Green represents fixed detection threshold and Red represents adaptive detection threshold.)

**Table 2** Statistics of cycle slip misjudgment rate at eight MGEX stations.

Date station	PRN (type) misjudge/total	PRN (type) misjudge/total	PRN (type) misjudge/total	PRN (type) misjudge/total	Success rate misjudge/total
2013/03/17	G24(MEO)	C01(GEO)	C07(IGSO)	C14(MEO)	0.16%
CUT0	0/820	5/2878	2/2341	1/882	8/6921
2013/03/17	G25(MEO)	C05(GEO)	C10(IGSO)	C14(MEO)	0.10%
REUN	0/795	4/2878	2/2259	1/904	7/6836
2013/03/17	G24(MEO)	G09(IGSO)	C10(IGSO)	C14(MEO)	0.67%
DLF1	1/780	4/1067	7/1025	14/1011	26/3883
2013/03/17	G24(MEO)	C01(GEO)	C09(IGSO)	C11(MEO)	0.30%
JFNG	3/690	8/2878	1/2128	8/1028	20/6724
2015/03/17	G03(MEO)	C01(GEO)	C07(IGSO)	C14(MEO)	0.17%
TUVA	5/1254	5/2878	2/2276	1/1221	13/7629
2015/03/17	G09(MEO)	C01(GEO)	C10(IGSO)	C14(MEO)	0.27%
XMIS	3/1025	7/2878	2/2878	9/923	21/7704
2015/03/17	G30(MEO)	C01(GEO)	C06(IGSO)	C14(MEO)	0.20%
NRMG	7/898	5/2878	2/2240	0/1129	14/7145
2015/03/17	G24(MEO)	C05(GEO)	C10(IGSO)	C14(MEO)	0.18%
DYNG	0/782	6/2878	2/1459	2/578	10/5697

violently within the range of (-0.08, 0.08) m, which conforms to the presence of the ionospheric disturbances phenomenon, and  $\Delta V I_1$  can be approximately regarded as a white noise sequence

with mean of zero. Although  $\Delta V I_1$  of MC05 reached -0.039 m at 22:25:30, it was caused by  $\Delta I_1$  of 0.024 m and -0.015 m at two adjacent epochs, which is far less than the influence of one cycle of slip. As a result,

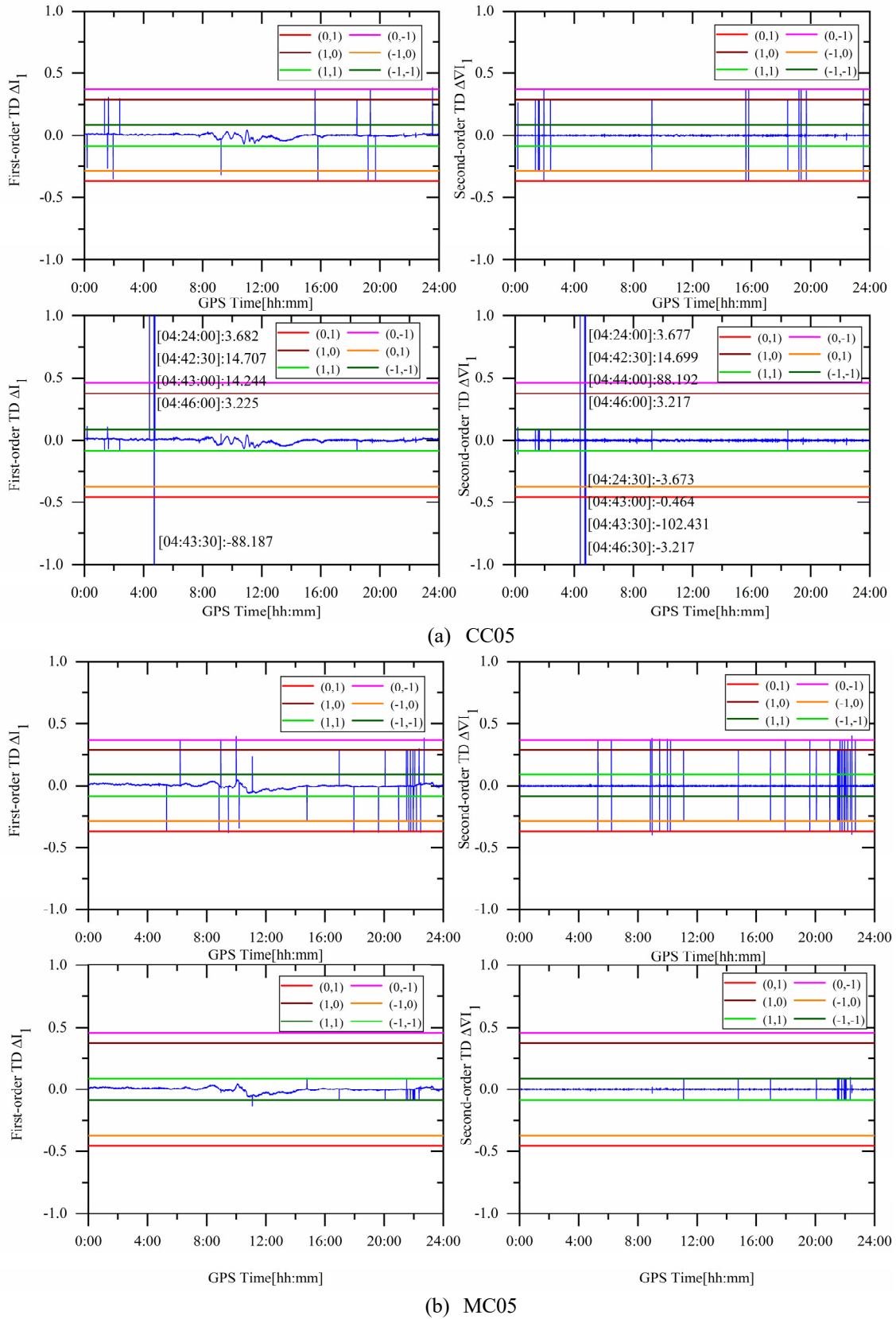


**Fig. 8** Residual ionospheric delay of CC05 and MC05 satellite before cycle slip repaired (Figures in each subfigure represent  $\Delta I_1^{12}$ ,  $\Delta V_1^{12}$ ,  $\Delta I_1^{13}$  and  $\Delta V_1^{13}$ , respectively. Different colors of horizontal lines represent the expected detection values when cycle slip on corresponding frequencies exists.)

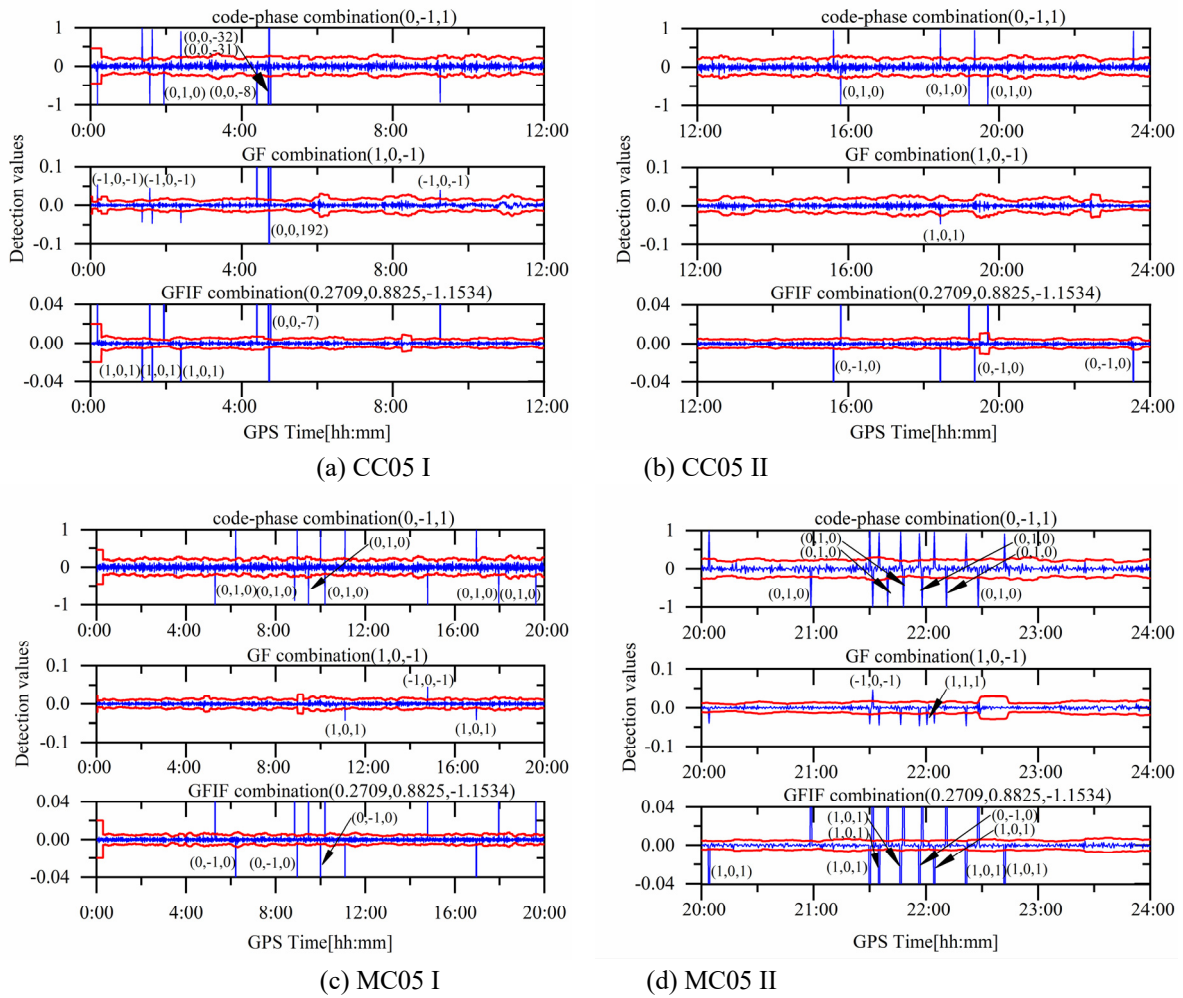


**Fig. 9** Detection and repair results for CC05 and MC05 (Blue represents detection values and Red represents adaptive detection threshold; figure (a) and (b) are for CC05, and figure (c) and (d) are for MC05).

19 real cycle slips of CC05 and 28 real cycle slips of MC05 were all correctly repaired, and the performance of the proposed algorithm was further verified.

### 5. CONCLUSIONS

Triple-frequency cycle slip detection and repair for GPS/BDS undifferenced observables under high ionospheric disturbances is the topic of this study. The proposed algorithm weakens the influence of ionospheric disturbances from three aspects: optimal observables combination, adaptive detection threshold and compensation for residual ionospheric delay. The proposed algorithm was tested using observables in geomagnetic storm periods at 9 MGEX stations. Results of simulated and real cycle slip detection and repair showed the proposed algorithm can process all kinds of cycle slips correctly under high disturbances with high reliability.

Note that the FNN used in this paper can be viewed as a kind of nonlinear fitter rather than a learner that need lots of training data. This is based on the short-term correlation principle of residual

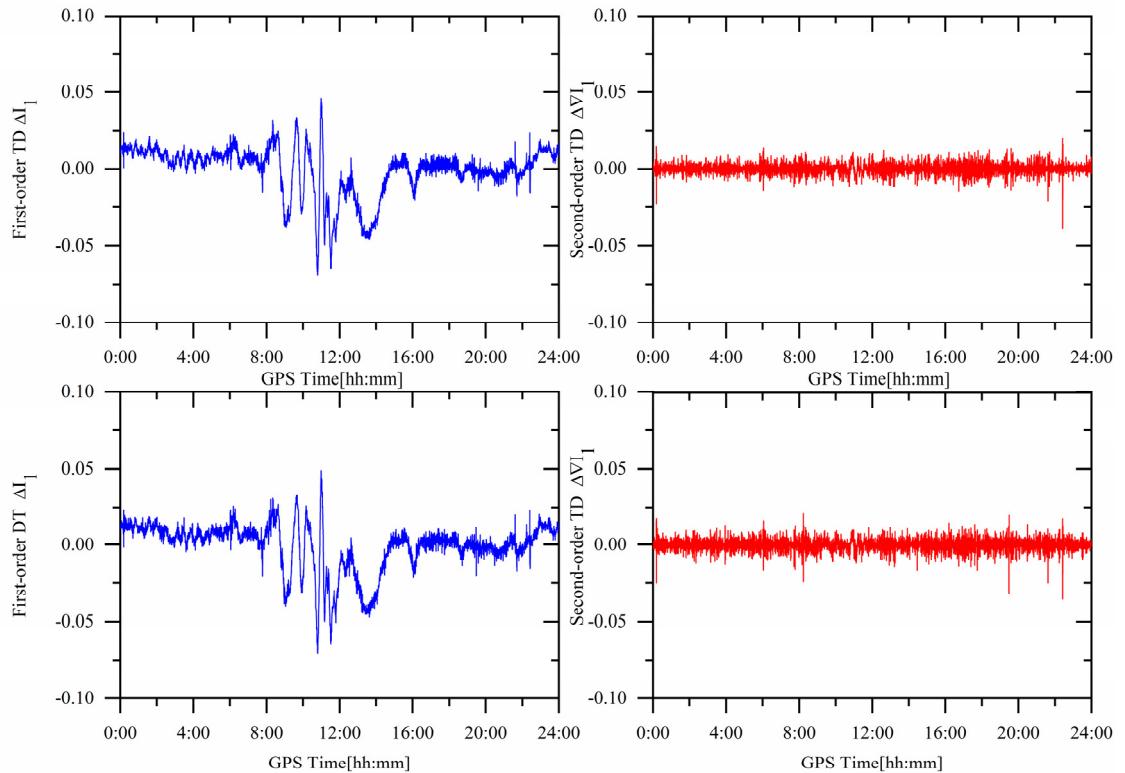
ionospheric delay. It should also be stressed that there are prices to pay for the success in dealing with cycle slips under high ionospheric disturbances, namely the complexity and computation of the proposed algorithm. However, MLAMBDA and FNN packages are out of the box, and this is not a problem for today's hardware.

### ACKNOWLEDGEMENTS

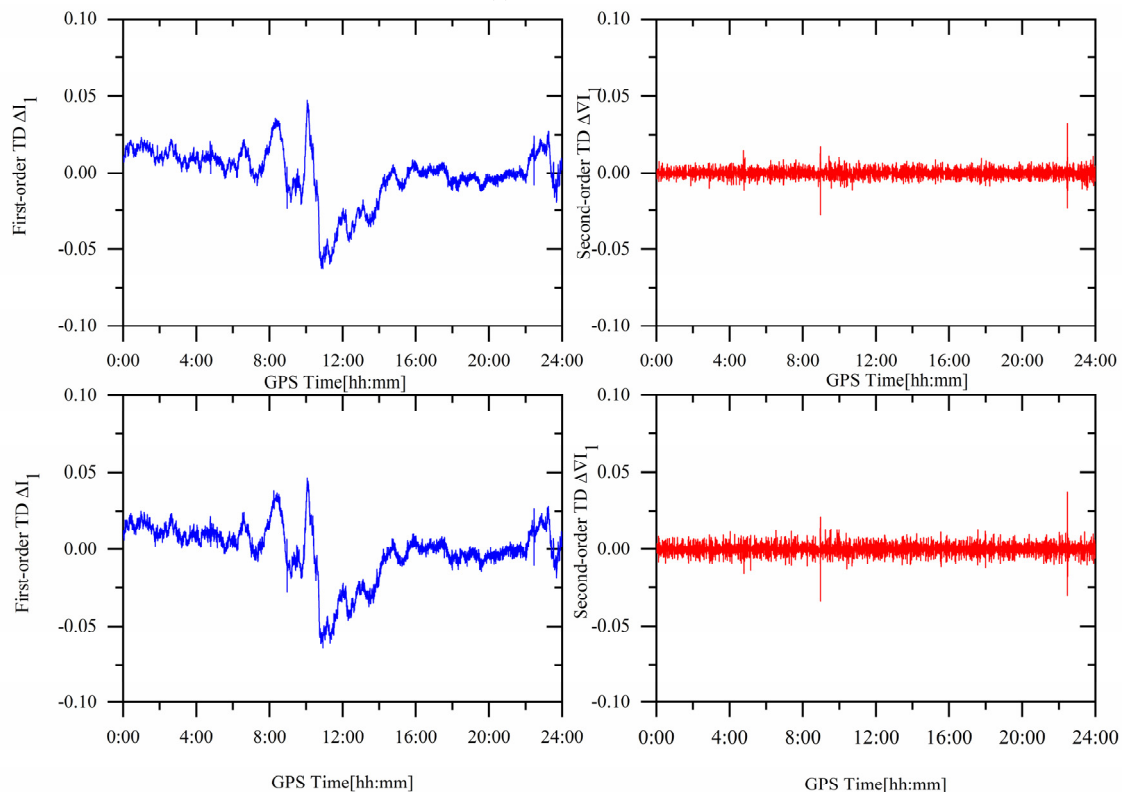
This work was supported by [the National Natural Science Foundation of China #1] under Grant [number 41974026, 41674008, 41774005], [China Postdoctoral Science Foundation #2] under Grant [number 2019M652010, 2019T120477] and [Postgraduate Research & Practice Innovation Program of CUMT #3] under Grant [number SJKY19\_1850].

### REFERENCES

Cellmer, S., Paziewski, J. and Wielgosz, P.: 2013, Fast and precise positioning using MAFA method and new GPS and Galileo signals. Acta Geodyn. Geomater., 10, 4, 393–400.  
DOI: 10.13168/agg.2013.0038



(a) CC05



(b) MC05

**Fig. 10** Residual ionospheric delay of CC05 and MC05 satellite after cycle slips are repaired (Figures in each subfigure represent  $\Delta I_i^{12}$ ,  $\Delta \nabla I_i^{12}$ ,  $\Delta I_i^{13}$  and  $\Delta \nabla I_i^{13}$ , respectively)

Chang, G.B., Xu, T.H., Yao, Y.F., Wang, H.T. and Zeng, H.E.: 2019, Ionospheric delay prediction based on online polynomial modeling for real-time cycle slip repair of undifferenced triple-frequency GNSS

signals. *Measurement*, 146, 289–297.

DOI: 10.1016/j.measurement.2019.06.036

Chang, G.B., Xu, T.H., Yao, Y.F. and Wang, Q.X.: 2018, Adaptive Kalman filter based on variance component estimation for the prediction of ionospheric delay in

- aiding the cycle slip repair of GNSS triple-frequency signals. *J. Geod.*, 92, 11, 1241–1253. DOI: 10.1007/s00190-018-1116-4
- Chang, X.W., Yang, X. and Zhou, T.: 2005, MLAMBDA: a modified LAMBDA method for integer least-squares estimation. *J. Geod.*, 79, 9, 552–565. DOI: 10.1007/s00190-005-0004-x
- Chen, J., Yue, D.J., Liu, Z.Q., Zhu, S.L. and Zhao, X.W.: 2018, Estimating the code bias of BDS to improve the performance of multi-GNSS precise point positioning. *Acta Geodyn. Geomater.*, 15, 4, 413–422. DOI: 10.13168/agg.2018.0031
- Chen, L.L. and Zhang, L.X.: 2016, Cycle-slip processing under high ionospheric activity using GPS triple-frequency data. In: *China Satellite Navigation Conference*, New York: 390, 411–423.
- Cocard, M., Bourgon, S., Kamali, O. and Collins, P.: 2008, A systematic investigation of optimal carrier-phase combinations for modernized triple-frequency GPS. *J. Geod.*, 82, 9, 555–564. DOI: 10.1007/s00190-007-0201-x
- Conker, R.S., El-Arini, M.B., Hegarty, C.J. and Hsiao, T.: 2003, Modeling the effects of ionospheric scintillation on GPS/Satellite-Based Augmentation System availability. *Radio Sci.*, 38, 1, 23. DOI: 10.1029/2000rs002604
- de Lacy, M.C., Reguzzoni, M. and Sanso, F.: 2012, Real-time cycle slip detection in triple-frequency GNSS. *GPS Solut.*, 16, 3, 353–362. DOI: 10.1007/s10291-011-0237-5
- Gao, X., Yang, Z.Q., Liu, Y. and Yang, B.: 2018, Real-time cycle slip correction for a single triple-frequency BDS receiver based on ionosphere-reduced virtual signals. *Adv. Space Res.*, 62, 9, 2381–2392. DOI: 10.1016/j.asr.2018.06.044
- Huang, L.Y., Lu, Z.P., Zhai, G.J. and Ouyang, Y.Z., Huang, M.T., Lu, X.P., Wu, T.Q. and Li, K.F.: 2016, A new triple-frequency cycle slip detecting algorithm validated with BDS data. *GPS Solut.*, 20, 4, 761–769. DOI: 10.1007/s10291-015-0487-8
- Ju, B., Gu, D.F., Chang, X., Herring, T.A., Duan, X.J. and Wang, Z.M.: 2017, Enhanced cycle slip detection method for dual-frequency BeiDou GEO carrier phase observations. *GPS Solut.*, 21, 3, 1227–1238. DOI: 10.1007/s10291-017-0607-8
- Kim, Y., Song, J., Kee, C. and Park, B.: 2015, GPS cycle slip detection considering satellite geometry based on TDCP/INS integrated navigation. *Sensors*, 15, 10, 25336–25365. DOI: 10.3390/s151025336
- Krzan, G. and Przeszelski, P.: 2016, GPS/GLONASS precise point positioning with IGS real-time service products. *Acta Geod. yn. Geomater.*, 13, 1, 69–81. DOI: 10.13168/AGG.2015.0047
- Li, B., Qin, Y. and Liu, T.: 2018, Geometry-based cycle slip and data gap repair for multi-GNSS and multi-frequency observations. *J. Geod.*, 93, No. 3, 399–417. DOI: 10.1007/s00190-018-1168-5
- Li, D.G., Ma, Z.Y., Zhao, J.M., Wei, Z. and Inst, N.: 2017, Cycle slips detection and correction of GPS/INS tightly integrated system based on Bayesian compressive sensing. In: *Proceedings of the 30th International Technical Meeting of the Satellite Division of the Institute of Navigation*, Washington, 3775–3783.
- Li, F., Gao, J., Li, Z., Qian, N., Yang, L. and Yao, Y.: 2019, A step cycle slip detection and repair method based on double-constraint of ephemeris and smoothed pseudorange. *Acta Geodyn. Geomater.*, 16, 4, 337–348. DOI: 10.13168/agg.2019.0028
- Li, H., Zhao, L. and Li, L.: 2016, Cycle slip detection and repair based on Bayesian compressive sensing. *Acta Phys. Sin.*, 65, 24, 8. DOI: 10.7498/aps.65.249101
- Li, X.X., Ge, M.R., Dai, X.L., Ren, X.D., Fritsche, M., Wickert, J. and Schuh, H.: 2015, Accuracy and reliability of multi-GNSS real-time precise positioning: GPS, GLONASS, BeiDou and Galileo. *J. Geod.*, 89, 6, 607–635. DOI: 10.1007/s00190-015-0802-8
- Liu, W.K., Jin, X.Y., Wu, M.K., Hu, J. and Wu, Y.: 2018, A new real-time cycle slip detection and repair method under high ionospheric activity for a triple-frequency GPS/BDS receiver. *Sensors*, 18, 2. DOI: 10.3390/s18020427
- Pu, R.H. and Xiong, Y.L.: 2019, An improved algorithm based on combination observations for real time cycle slip processing in triple frequency BDS measurements. *Adv. Space Res.*, 63, 9, 2796–2808. DOI: 10.1016/j.asr.2018.08.011
- Qian, N.J., Chang, G.B. and Gao, J.X.: 2019, GNSS pseudorange and time-differenced carrier phase measurements least-squares fusion algorithm and steady performance theoretical analysis. *Electron. Lett.*, 55, 23, 1238–1240. DOI: 10.1049/el.2019.2408
- Rocken, C., Johnson, J.M., Braun, J.J., Kawawa, H., Hatanaka, Y. and Imakiire, T.: 2000, Improving GPS surveying with modeled ionospheric corrections. *Geophys. Res. Lett.*, 27, 23, 3821–3824. DOI: 10.1029/2000gl012049
- Teunissen, P.J.G. and de Bakker, P.F.: 2013, Single-receiver single-channel multi-frequency GNSS integrity: outliers, slips, and ionospheric disturbances. *J. Geod.*, 87, 2, 161–177. DOI: 10.1007/s00190-012-0588-x
- Tian, Y.J., Sui, L.F., Zhao, D.Q., Tian, Y., Feng, X. and Qu, M.Y.: 2019, Performance of BDS triple-frequency positioning based on the modified TCAR method. *Surv. Rev.*, 1–8. DOI: 10.1080/00396265.2019.1627507
- Wu, X.L., Hu, X.G., Wang, G., Zhong, H.J. and Tang, C.P.: 2013, Evaluation of COMPASS ionospheric model in GNSS positioning. *Adv. Space Res.*, 51, 6, 959–968. DOI: 10.1016/j.asr.2012.09.039
- Wu, Y., Jin, S.G., Wang, Z.M. and Liu, J.B.: 2010, Cycle slip detection using multi-frequency GPS carrier phase observations: A simulation study. *Adv. Space Res.*, 46, 2, 144–149. DOI: 10.1016/j.asr.2009.11.007
- Yao, F., Gao, J.X., Wang, J., Hu, H. and Li, Z.K.: 2016, Real-time cycle-slip detection and repair for BeiDou triple-frequency undifferenced observations. *Surv. Rev.*, 48, 350, 367–375. DOI: 10.1080/00396265.2015.1133518
- Yu, J.Y., Yan, B.F., Meng, X.L., Shao, X.D. and Ye, H.: 2016, Measurement of bridge dynamic responses using network-based real-time kinematic GNSS technique. *J. Surv. Eng.-ASCE*, 142, 3, 12. DOI: 10.1061/(asce)su.1943-5428.0000167
- Zangeneh-Nejad, F., Amiri-Simkooei, A.R., Sharifi, M.A. and Asgari, J.: 2017, Cycle slip detection and repair of undifferenced single-frequency GPS carrier phase observations. *GPS Solut.*, 21, 4, 1593–1603. DOI: 10.1007/s10291-017-0633-6
- Zeng, T., Sui, L.F., Xu, Y.Y., Jia, X.L., Xiao, G.R., Tian, Y. and Zhang, Q.H.: 2018, Real-time triple-frequency cycle slip detection and repair method under ionospheric disturbance validated with BDS data. *GPS Solut.*, 22, 3, 13. DOI: 10.1007/s10291-018-0727-9
- Zhang, X.H. and Li, P.: 2016, Benefits of the third frequency signal on cycle slip correction. *GPS Solut.*, 20, 3, 451–460. DOI: 10.1007/s10291-015-0456-2